ELSEVIER

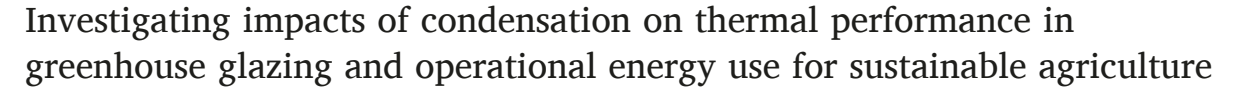
Contents lists available at ScienceDirect

Biosystems Engineering

journal homepage: www.elsevier.com/locate/issn/15375110



Research Paper



Enhe Zhang a, Md Anwar Jahid a,b, Julian Wang a,b,*, Nan Wang a, Qiuhua Duan c

- ^a Department of Architectural Engineering, Pennsylvania State University, University Park, PA, 16802, USA
- ^b Materials Research Institute, Pennsylvania State University, University Park, PA, 16802, USA
- ^c Department of Civil, Construction, and Environmental Engineering, The University of Alabama, Tuscaloosa, AL, 35487, USA

ARTICLE INFO

Keywords: Energy efficiency Environmental-controlled agriculture Condensation effect U-factor Emissivity Wettability

ABSTRACT

Condensation frequently manifests in environmentally controlled agricultural structures (such as greenhouses) due to the utilisation of specific covering materials and the often meticulous management of high relative humidity to facilitate optimal plant growth. The formation of condensation can significantly influence the thermal and optical characteristics of the covering materials, which also affects the covering insulation and the growth of plants. This study was conducted to investigate the impacts of surface condensation on the thermal performance of various greenhouse covering types. These options feature low-emissivity (Low-E) coatings, infrared reflective (IR) additives, UV protective films, and anti-condensation additives. The physical properties, specifically emissivity and wettability, were examined to understand their roles in modifying the thermal transfer dynamics of greenhouse coverings. A scale physical model was made to test the thermal performance of the coverings with and without condensation. The results indicated the effect of condensation on the overall heat transfer coefficient (U-factor). Especially when the surface exhibited characteristics of low emissivity, it resulted in a notable neartripling of the U-factor. These widely accepted and advocated strategies of Low-E and IR reflective products may inadvertently lead to enhanced operational energy consumption when considering the influence of condensation. Notably, this research has also devised a regression function that establishes a correlation between the contact angle and the condensation heat transfer coefficient. This tool facilitates swift analysis and estimation of the effects of condensation on the U-factor. In the end, the potential and future work on condensation effects is also discussed.

1. Introduction

More than 55 countries worldwide are currently using greenhouse technology for crop cultivation. The total covered area was estimated to be over 4.09 billion m² in 2018 (Sahdev, Kumar, & Dhingra, 2019). The total covering area of greenhouses and high tunnels in America is about 83.0 million m². From the energy consumption perspective, 65%–85% of the total energy used in greenhouses is for heating, accounting for 60%-72% of total greenhouse operation costs (Ahamed, Guo, & Tanino, al.. 2019: Gorijan et 2021). In high latitudes. environmentally-controlled greenhouses with glass covers consume about 1100 to 1900 MJ m⁻² per year, and worldwide more than 880 PJ per year (Katzin, Marcelis, & van Mourik, 2021). Recently, scholars have begun developing and studying ways to reduce heating and cooling energy costs in conventional greenhouse cover materials and designs,

including solar-integrated energy-efficient designs such as optimisation orientations, shades, and shapes (Dragićević, 2011; Ghasemi Mobtaker, Ajabshirchi, Ranjbar, & Matloobi, 2016; Singh & Tiwari, 2010), innovative coverings such as anti-reflective coatings, solar PV-integrations, and solar thermal collectors (Fabrizio, 2012; Hassanien, Li, & Yin, 2018; Vitkin et al., 2020; Yano & Cossu, 2019), lighting supplies with heating features (Kuijpers et al., 2021; Yang, Lee, Ashtiani-Araghi, Kim, & Rhee, 2015), and the energy efficiency of heating systems such as solar powered HVAC heating and thermal energy storage (Agrebi, Chargui, Tashtoush, & Guizani, 2021; Fabrizio, 2012; Skarphagen, Banks, Frengstad, & Gether, 2019).

Among those studies, covering materials have attracted significant attention among these strategies because the coverage system is essential to a greenhouse's heat exchange with solar sources and the ambient environment. Two major types of covering materials are glasses and plastics, while glass materials continue to hold prominence in the

^{*} Corresponding author. Department of Architectural Engineering, 104 Engineering Unit A, The Pennsylvania State University, University Park, PA, 16802, USA. *E-mail address*: julian.wang@psu.edu (J. Wang).

Nomenclature		A k	Area, m ² Thermal conductivity, W⋅m ⁻² K ⁻¹
Symbols		L	Z-dimensional length, m
Q _{total}	Overall heat transfer, W	ρ	The density of liquid, kg·m ⁻³
Q _{e,tol} U _{total}	Overall heat transfer in experiments, W Overall heat transfer coefficient, $W \cdot m^{-2}K^{-1}$	ρ _v g	The density of vapour, $kg \cdot m^{-3}$ Gravitational constant, $m^3 \cdot kg^{-1}s^{-2}$
$l_{c,expr}$	Condensation heat transfer coefficient (experimental), $W \cdot m^{-2} K^{-1}$	μ	Dynamic viscosity, kg⋅m ⁻¹ s ⁻¹
$h_{c,doub}$	Condensation heat transfer coefficient (double film theoretical), $W \cdot m^{-2} K^{-1}$	Abbreviat UV	Ultraviolet
\mathbf{l}_c	Condensation heat transfer coefficient, conventional/one film theory $W \cdot m^{-2} K^{-1}$	RH HVAC	Relative humidity Heating, Ventilation, and Air Conditioning
R _{specimen} Ti	Specimen thermal resistance, m ² K·W ⁻¹ Inner space temperature, °C	ASHRAE NIR	American Society of Heating and Air-Conditioning Engineers Near-infrared
Γ_o Γ_{gi}	Ambient temperature, °C Specimen inner surface temperature, °C	Low-E U-factor	Low emissivity
T_{go} Hv	Specimen outer surface temperature, $^{\circ}$ C Latent heat of evaporation, kJ·kg $^{-1}$	CA	Contact angle

context of standard greenhouses and other agricultural establishments (Maraveas, 2019; Reddy, 2016). Their enduring popularity can be attributed to their construction and maintenance efficiency, encompassing radiometric and thermal properties as well as extended functional longevity (Maraveas, Kotzabasaki, Bayer, & Bartzanas, 2023; Papadakis et al., 2000; Teitel, Vitoshkin, Geoola, Karlsson, & Stahl, 2018). Research has shown that the glazing system is responsible for 20%–40% of the energy used in the general civic building environment (Goetzler, Guernsey, & Young, 2014; Katzin et al., 2021; Li et al., 2022). In comparison to conventional building environments, the potential for energy wastage can be even more pronounced within greenhouse facilities. Notably, recent years have witnessed the emergence of diverse glazing technologies tailored for greenhouse contexts aimed at augmenting operational energy efficiency. Nevertheless, despite these advancements, the prevailing glazing options largely encompass conventional single-pane horticultural glass, double-pane configurations, and low-emissivity (Low-E) coated glazing. Of these, double-pane glazing stands out, capable of yielding energy savings between 40% and 50%, accompanied by a mere 10% reduction in solar transmissivity (also energy receiving reduction) when compared to its single-pane horticultural glass counterpart (Papadakis et al., 2000). Furthermore, when Low-E products (e.g., adhesive films, thin layers) are added, the energy-saving potential can be above 60% relative to single-pane horticultural glass (Max et al., 2012). Corresponding to the Low-E technologies, infrared (IR) reflective additives are also integrated into plastic films to prevent harmful IR radiation. Plus, stabiliser additives are also used to absorb UV radiation (Maraveas, 2019). Overall, it has been accepted that IR-reflective additives and Low-E coated glass outperform other covering materials from the greenhouse's operational energy use perspective by reflecting unwanted IR radiation (Papadakis et al., 2000).

Within the realm of architectural windows and building envelopes, a growing corpus of empirical data has underscored the role of Low-E and IR-reflective surfaces in diminishing the condensation resistance of glazing installations. This, in turn, exerts adverse repercussions on diverse aspects encompassing heat exchange dynamics, material longevity, solar transmittance, and related factors. In the unique context of greenhouse environments, the propensity for condensation is even more pronounced due to the imperative maintenance of an ambient inner air relative humidity (RH) range of 60%–80% (Amani, Foroushani, Sultan, & Bahrami, 2020). In contrast with the optimal humidity range upheld in residential dwellings (typically between 40% and 60%), the proclivity for condensation to manifest on glazing surfaces within greenhouse environments is notably heightened.

As shown in Table 1, a variety of studies have been conducted to

investigate the impact of condensation on greenhouse environments. In particular, Pieters and Deltour (1997) calculated the greenhouse heating load with and without condensation for four different types of greenhouse coverings and found that the presence of condensation increased the auxiliary heating requirement by 6.7%-17.5%, due to the effect on the surface temperature of the covering materials. Feuilloley and Issanchou (1996) determined the effects of condensation on glass and plastic glazing and identified correlations between the heat transfer of condensation and variables such as air temperature differences, surface transmittance, airflow velocity, and sky temperature. They formulated six balance equations and solved them using matrix algebra. Pollet and Pieters (1999, 2000a, 2000b) studied the solar radiation transmittance of glass and plastic samples with and without condensation and found no significant effect of condensation on transmittance. They also investigated the effect of condensation on photosynthetically active radiation (PAR) transmission in 2002 and obtained similar results, suggesting that condensate water only slightly alters the transmittance spectrum (Pollet & Pieters, 2002). However, the findings of Al-Kayiem et al. (2019) conflicted with those Pollet and Pieters found. They conducted an outdoor canopy test with a condensation film and found an 8%-13% reduction in solar transmittance due to the presence of condensation. Comparatively, although the heat transfer issue is significant to operational energy use in greenhouse facilities, few studies have been conducted on the thermal transfer effects resulting from water condensation occurring on the inner surfaces of greenhouse covering, especially for the radiometric property of the material.

In most situations, the condensate surface is in a hybrid mode that combines the original surface and condensate surface (both filmwise and dropwise). This means that emissivity values (for the original and condensate surfaces) may be involved in the resulting thermal insulation. Recent research by Troseille et al. (2022) has examined the influence of water droplets on the effective emissivity of greenhouse surfaces and discovered a critical threshold of droplet thickness between 12 and 20 µm, beyond which the droplets effectively contribute to surface emissivity. Another study on the emissivity of condensation discovered that the emissivity of a reflective aluminium surface grows rapidly with an increase in the surface density of the condensation. Conversely, the condensate surface film's emissivity thickness-dependent and fundamentally influenced by surface wettability.

Elsewhere, the surface contact angle formed between a liquid meniscus and its intersected solid surface represents the surface's wettability and determines the thickness of the condensate surface film. Prior works have studied such measurements and concluded that the

Table 1Previous studies on condensation in greenhouse facilities.

Research goal	Condensation affects	Method	Reference
To study the influence of water condensation on the effective emissivity of the greenhouse surface.	mean surface emissivity	Emissivity measurements during condensation events using IR camera.	Trosseille, Mongruel, Royon, and Beysens (2022)
To compare overall heating loads for the greenhouse with or without condensation	vegetation temperature. air temperature.	Simulations using Gembloux Greenhouse Dynamic Model (G.G.D.M.)	Pieters and Deltour (1997)
To determine the effect of condensation on the heat transfer coefficient of plastic films and glass	U-factor	Experiments using the isothermal hot box method with various covering materials. Also include water mass measurements and validate with a computational model.	Feuilloley and Issanchou (1996)
To determine the radiation transmittances of two samples (PE and glass), including the effect of water condensation.	solar transmittance	Using laser beams as light source and measuring solar transmittance during distinct phases of covering materials.	(Pollet & Pieters, 1999; 2000a; 2000b)
To determine PAR transmittance as a function of incident angle and wavelength. (Glass, Low-E, PE plastic)	PAR transmittance	Using a laser beam as a light source, measure PAR (400 nm–700nm) transmittance for various cladding materials.	Pollet and Pieters (2002)
To determine the effect of condensate film on solar chimney performance (solar radiation transmittance).	solar transmittance	Using a solar chimney model and data collection for one month.	Al-Kayeim, Aurybi, and Gilani (2019)
To investigate the mean heat transfer resistance of the condensate droplets which form on the substrate surface.	mean condensation layer heat transfer coefficient (h_d)	Experiments using heat flux measurements and thermography (IR camera) recording to calculate heat transfer coefficient.	Eimann, Zheng, Philipp, Fieback, and Gross (2018)
To present a mathematical model for dropwise condensation heat transfer prediction of superhydrophobic surface	heat flux	A developed single drop heat transfer model with drop size distribution and predict overall heat transfer rate per unit area (heat flux).	Kim and Kim (2011)

dropwise condensation heat transfer coefficient heavily depends on the contact angle for different surfaces. Neumann, Abdelmessih, and Hameed (1978) used well-polished copper as a substrate and found a strong relationship between contact angle hysteresis and a decrease in the heat transfer flux and coefficient. Rosengarten, Cooper-White, and Metcalfe (2006) examined the effects of contact angle on convective heat transfer in microchannels, finding that contact angle is an essential consideration for laminar flow/heat in micro- and nano-heat exchanger design. Kim and Kim (2011) developed a mathematical model to predict the heat transfer coefficient of dropwise condensation on a superhydrophobic surface. They proposed a model prediction of overall heat flux with consideration of droplet distribution beyond a single-drop heat

transfer model. However, the model only showed up to $10~^{\circ}$ C temperature differences for filmwise condensation and narrowed the contact angle range from 90° to 150° for dropwise condensation.

As outlined in the preceding sections, the persistent issue of greenhouse condensation has notable implications for plant growth and energy consumption. However, much of the existing research has centred on the impacts of condensation on individual materials, neglecting a more comprehensive approach. Although some studies have indeed considered a range of materials, their primary focus has been the influence of condensation on solar transmittance rather than on overall heat transfer dynamics. Consequently, the interrelationships and effects of surface properties of various materials on condensation heat transfer remain inadequately understood. This knowledge gap inhibits the proper selection of the greenhouse covering materials, especially considering the potential implications for operational energy use under conditions with and without condensation. An additional significant obstacle resides in the fact that prior research efforts have individually validated mathematical models for condensation heat transfer, but these validations were conducted under a restricted set of simulated environments or material types. This has resulted in the production of divergent coefficients and factors across these studies. Consequently, the lack of consistent and definitive mathematical models for condensation heat transfer applicable to greenhouse facilities hinders future heat transfer and energy simulations.

To address the aforementioned challenges, the design conducted meticulous experiments utilising an environment chamber and hotbox experimental setup. These experiments, conducted with strict control over temperature, wind speed, and humidity, scrutinised the effects of surface condensation on several representative greenhouse glazing materials. The research emphasised filmwise condensation due to its prevalence in engineering applications and its characteristic formation on vertical surfaces (Eimann et al., 2018). Through this comprehensive experimental approach with different material samples, the design aimed to augment comprehension of the dynamics of surface condensation and its interplay with greenhouse glazing surfaces. Specifically, this study made two notable contributions:

Firstly, this research endeavoured to investigate the influences of surface condensation on thermal transfer performance, considering the variability in glazing surface properties such as emissivity and wettability, as well as varying environmental thermal conditions. Various technologies and products are presently deployed in greenhouse coverings to enhance energy efficiency and curtail condensation. Nonetheless, their actual effectiveness and collective impact on overall heat transfer during the condensation process remain to be clearly understood. This study explicitly delineates the variations in overall heat transfer before and after the onset of condensation via experiments and scrutinises the associated relationships and influences of different material surface properties. By shedding solar light on these relationships and the effects these surface properties exert on the condensation heat transfer coefficient, the study can facilitate a more accurate estimation of their energy performance. This will significantly inform the design process and material selection for greenhouse coverings.

Secondly, this study aimed to identify and validate key coefficients necessary for analytical condensation heat transfer coefficient calculations. Despite condensation being a routine phenomenon in greenhouse facilities, there is an existing need for an effective analytical methodology to quantify its effects on overall heat transfer coefficient and energy consumption. The validated model, generated as part of this research, will facilitate more accurate analytical analyses and computation of the implications of condensation on heat transfer coefficient, thereby allowing its integration into broader energy simulations.

The remainder of this work is organised as follows. Section 2 presents the experimental setup used in the lab and the selected representative greenhouse glazing samples' thermal and wettability characteristics. Section 3 contains the results obtained from the condensation and thermal transfer tests and an analysis of the influence of the surface

properties (i.e., emissivity and contact angle) on the condensation heat transfer coefficients. Section 4 addressed the physical basics, along with the discussions about the findings and future improvements. At last, the conclusions are presented in Section 5.

2. Experimental investigation

2.1. Experiment setup

To study condensation on the inner surface of a greenhouse, an experiment was conducted using a facility located in Engineering Unit A at Penn State University - Park Campus. The facility consisted of an environment chamber that measures 3.6 m \times 4.0 m, with independent control over airflow rate, temperature, and indoor/outdoor air exchange and mixing. Using the hotbox method (Asdrubali & Baldinelli, 2011; Friman Peretz et al., 2019; Rabiu et al., 2022) allowed the maintenance of the outdoor conditions, while indoor temperature and humidity control were achieved through a physical model placed in the chamber. The hot box method using the physical model, referred to as the "test box," was made from an ultra-insulated polyurethane container with 5.1 cm polyurethane insulation and one side opening of 45.8 cm \times 45.8 cm and 45.8 cm deep. And the specimens' thermal properties at one opening of the box are tested using standardised measurements. The key for this method of using the test box was the highly insulated walls (negligible heat transfer through thick "wall" insulation) and an only opening which is also well sealed with the sample specimens to ensure that heat transfer only occurred through the opening that was covered by the selected specimen. Fig. 1 shows a schematic diagram and pictures of the experimental apparatus used to study the vertical surface condensation heat transfer coefficient performance.

As shown in Fig. 1 IV, the sensors and equipment are listed below.

From left to right, a 120V and 750W silicone-heated pad (Richoose 31 cm \times 31 cm) was placed at Position 3 (fully covered "back wall") for the test box heating process. The heating temperature was controlled using an automatic system with a temperature sensor ($-50~{\rm ^{\circ}C-70~^{\circ}C\pm1~^{\circ}C}$) and switch. To control the relative humidity (RH) inside the box, A miniature humidifier system (AGPtEK Mist Maker) at Position 2 (25 cm away from the sample surface) was used to moisture the inner space, which was manually controlled from an external terminal (computer at Position 10). During the experiments, the "outdoor temperatures" were maintained at a constant level using the environment chamber while continuously monitoring and controlling the "indoor temperatures" and "RH" to enable thermal transfer measurements with relatively stable filmwise-focused condensation on the inner surface of the glazing. In content, outdoor means the inner space of the environment chamber, and indoor represents the inner space of the test box.

The measurement systems used in the experiment consisted of wireless/wired environmental sensors, heat flux sensors, and a data logger to measure the environmental variables. The HOBO environmental sensors network and GreenTEG temperature sensors were used to measure temperature and RH. A HOBO analogy/temp/RH/light data logger (± 0.20 °C from 0° to 50 °C) was placed outside and close to the physical model, for the evaluation of the ambient temperature at Position 9. The HOBO temp/RH sensors for temperature and humidity measurements were placed at Position 1 (15 cm down the ceiling and 25 cm away from the samples, model S-THC-M002, RH: 10%– $90\% \pm 2.5\%$, Temperature: 0 °C–70 °C \pm 0.20 °C), with each sensor on every surface of the specimen to measure interior and exterior surface temperatures at Position 6 and 8 (Air Temperature Sensor, model TMCI-HD, Temperature: 0 °C–50 °C \pm 0.21 °C). A temperature sensor from GreenTeg (GreenTEG gSKIN® U-Value KIT, Temperature: 10 °C–125 °C \pm 0.5 °C) was used to measure the surface air temperatures for the air/air-vapour-

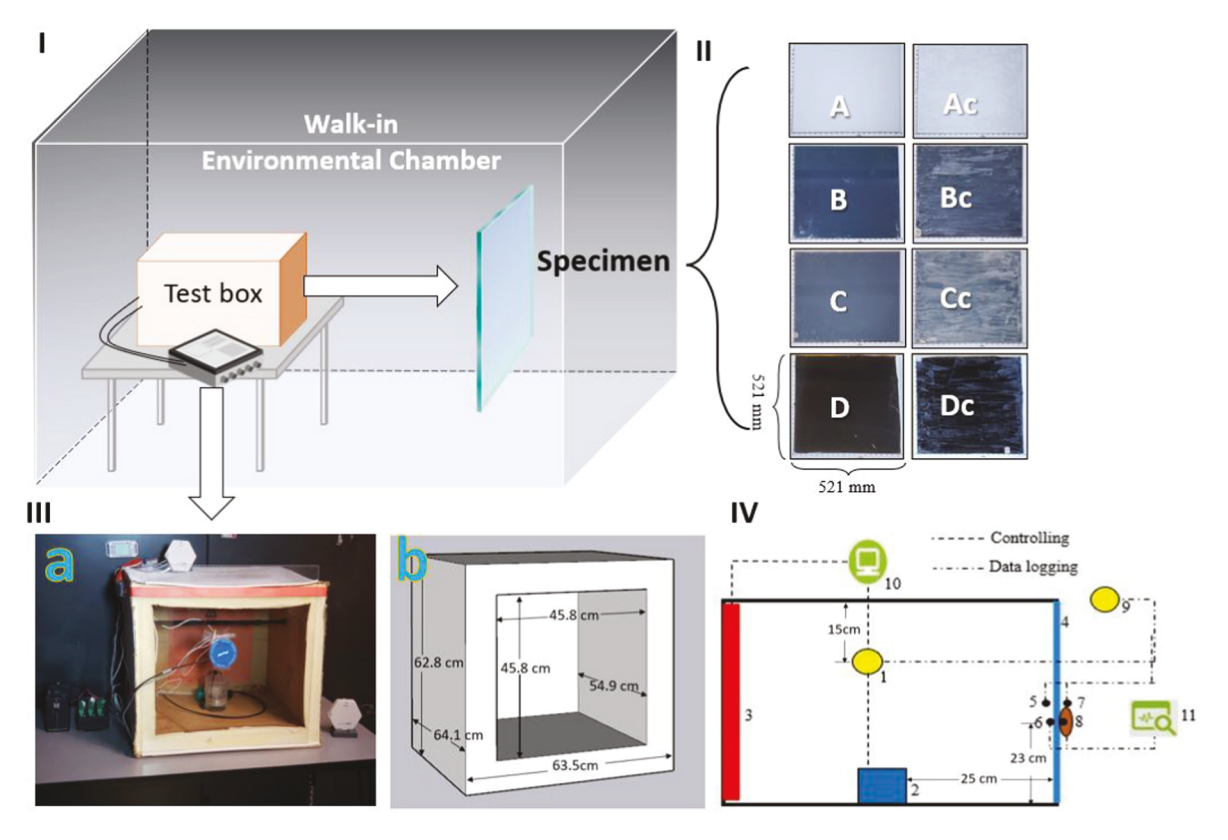


Fig. 1. Experiment setup. (I) The environment chamber and physical model layout. (II-IV) Schematic view of the physical model. (II) Figures of the specimens. A. Clear glass. Ac. Clear glass coated with anti-condensation. B. Film Low-E20. Bc. Film Low-E20 coated with anti-condensation. C. Film Low-E35. Cc. Film Low-E35 coated with anti-condensation. D. UV. Dc. UV coated with anti-condensation. (III)a. Front view of the set with clear glass. b. Dimension layout. (IV)1. HOBO S-THC-M002. 2. Humidifier. 3. Heating pad. 4. Specimens. 5&7. GreenTEG temperature sensors. 6&8. HOBO air temperature sensor and Hukseflux HFP. 9. HOBO analogy/temp/RH/light data logger. 10. Computer and software. 11. HOBO and Campbell scientific data logger.

liquid mixtures at Position 5 and 7. This sensor was placed 2.5 cm from the surface. To measure the heat flux through the glazing layer, a heat flux sensor (Hukseflux HFP, $-2000~W~m^{-2}$ to $2000~W~m^{-2}\pm3\%$) was attached to the glazing surface, next to the temperature sensors at Position 8. The "outdoor airflow speed" was monitored using a Testo 440 air velocity meter ($\pm0.5\%$ of mv) close to Position 8. The study continuously documented all data throughout the experiment, from the no-condensation stage to the filmwise condensation stage and the falling droplet stage (further explained in section 2.2.1), using a datalogger (Campbell scientific data logger CRX1000, equipment Position 11) and extracted it from the related computer program (PC400 and gSKIN@ Uvalue software, computer Position 10). The tested sample was placed and sealed through Position 4 to fully block the opening of the test box.

2.1.1. Experimental procedure

In order to repeat the experiment and to introduce the procedure of the hotbox method, they are described in the following paragraphs. This study aimed to investigate the heat transfer behaviour of filmwise condensation in a testing box across three distinct ambient temperature ranges. The following stages are shown in Fig. 2. The experiment was conducted over 300 min and comprised three stages: a preparation stage (from 0 to 60 min) at 24 $^{\circ}$ C, a cooling stage (60–240 min) from 35 $^{\circ}$ C to 25 °C, and a heating stage (240–300 min) from 25 °C to 35 °C. The ambient temperature was held at 24 °C during the preparation stage while the inner space of the test box was heated to 50 °C. Moisture was then slowly added until the RH reached 60%. At this point, no condensate had yet formed on the testing substrate. In the first cooling stage, the ambient temperature decreased uniformly from 35 °C to 25 °C, while the test box was maintained at a high RH of 60% and temperature of 50 °C. As a result of the temperature difference between the test box and the interior sample surface, condensation formed on the interior surface of the specimen, and dropwise condensate also appeared. In the second heating stage, the test box began at 60% RH and inner space temperature at 50 $^{\circ}$ C, while the ambient (outer) temperature was 25 °C. Filmwise condensation was observed at this point. The ambient temperature was then uniformly increased from 25 $^{\circ}\text{C}$ to 35 $^{\circ}\text{C}\text{,}$ while the test box was held at its current condition of temperature and RH. As the temperature difference between inner and outer space

decreased, the condensation slowed and eventually disappeared. The heaters and coolers were then turned off, and the system was allowed to cool naturally to room temperature till no water condensate was observed on the specimen. This procedure was repeated for each specimens, and the air velocity near the glazing surface was maintained at $0.03~{\rm m~s^{-1}}$ during all processes, which is considered still air. The study findings were recorded and analysed using various measurement tools such as heat flux sensors, temperature sensors, and a data logger.

Fig. 2 depicts a prototypical test procedure for a glass specimen, where data were collected and recorded at 1-min intervals. The inner box space temperature was maintained throughout the process. A surface film heat transfer coefficient of the sample, as shown on the vertical axis of Fig. 2, was determined by calculating the parameters measured from the heat flux sensor and temperature probes, the determination of surface film heat transfer coefficient with and without condensation is equivalent and outlined in Section 2.4. During Phase 1, the heat transfer coefficient increased with an increase in relative humidity (%RH), transforming the dry air film on the inner surface of the sample into an air and moisture mixture. In Phase 2, the ambient temperature, simulating the outdoor environment, decreased, while the inner temperature and humidity remained constant. As a result, the interior surface temperature decreased, causing condensation to form on the surface once the dew point temperature reached. This fog eventually formed a relatively stable thin film layer, which is illustrated in Fig. 2 during Phase 2. The heat transfer coefficient increased rapidly due to the onset of film condensation, which constituted the primary focus of the analysis. In Phase 3, the cooling process was reversed to a heating process, causing the sample surface temperatures to increase, resulting in condensation's disappearance. The heat transfer coefficient decreased rapidly, eventually returning to its original level.

2.1.2. Uncertainty

In this study, all the tests were performed at atmospheric pressure. The test box was well insulated, and the glass sample was sealed with a thermal insulation tap to minimise heat loss and air leakage. Measurement accuracy was introduced in section 2.1 with the experiment setup. Due to the rather small capacity of the test box, the inner temperature and humidity can be considered constant. The uncertainty in the single-

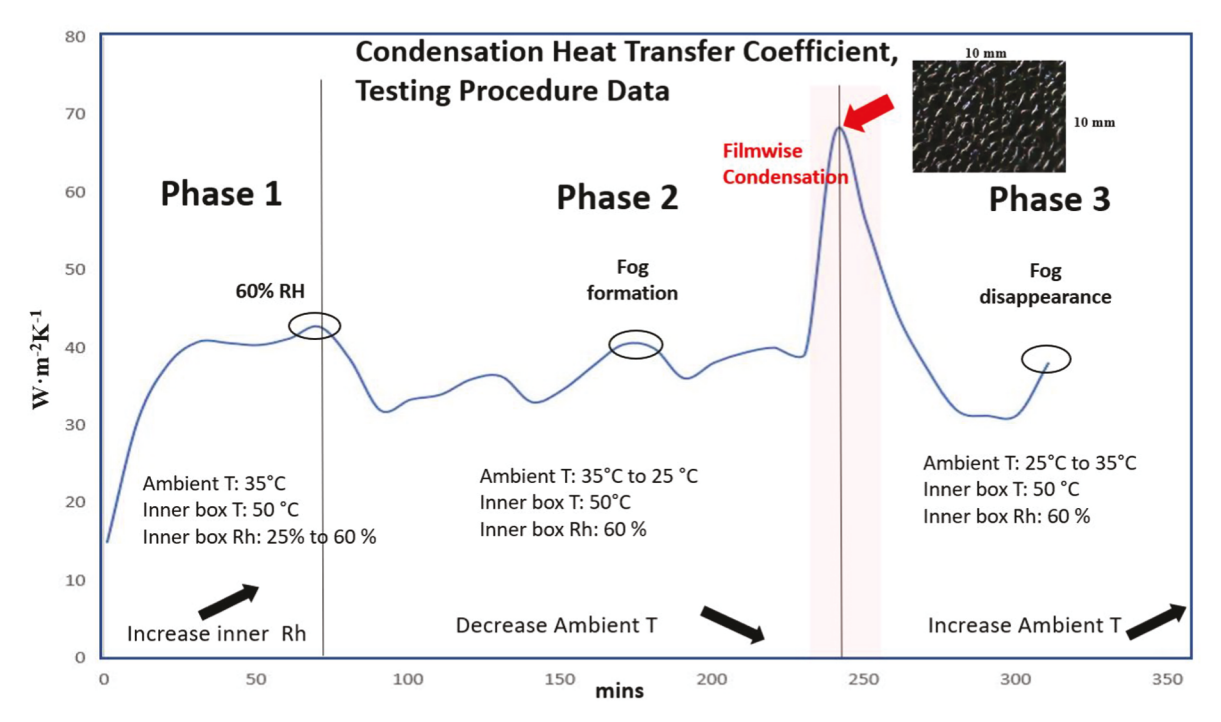


Fig. 2. Experiment procedure.

sample experiments was carried out using the method suggested by Moffat (1985). The typical uncertainties in the calculated condensation heat transfer coefficients were estimated to be less than $\pm 5\%$. As the case stands, these uncertainties are basically reasonable and acceptable since some unpredictable uncertainties may always exist during the experiments.

2.2. Characterisation of greenhouse glazing materials

Eight different glazing samples were prepared. The most basic sample was a clear glass plate that was also used as a substrate to obtain the other three specimens: clear glass with UV block adhesive film (UV), Low-E20 coated glass (L20), and Low-E35 coated glass (L35). The clear glass samples were borosilicate glass plates from GO-3D PRINT (51 cm × 51 cm x 3 mm). UV (Snapguard Solutions, 25% visible), L20 (3M™ Low-E), and L35 (3M™ Low-E) films were applied on each clear glass plate via a certified window coating manufacturer - PA Window Tint, Inc. We prepared two sets of the above four specimens. One set was then sprayed with an anti-condensation (AC) agent (SunClear from Greenhouse Megastore), following the Greenhouse Megastore spraying instructions. As a result, the other four samples were obtained, including clear glass coated with anti-condensation (CGAC), L20 coated with anticondensation (L20AC), L35 with anti-condensation (L35AC), and UV coated with anti-condensation (UVAC). All materials and chemicals prepared and used above are typically and widely adopted in the current practices of the greenhouse covering materials.

X-ray photoelectron spectroscopy experiments were performed to understand the major elemental composition of the coatings/films used on the clear glass substrate. These were accomplished using a Physical Electronics VersaProbe III instrument equipped with a monochromatic Al $k\alpha$ x-ray source ($h\nu=1486.6$ eV) and concentric hemispherical analyser. Charge neutralisation was performed using low-energy electrons (<5 eV) and argon ions. The binding energy axis was calibrated using sputter-cleaned Cu (Cu 2p3/2 = 932.62 eV, Cu 3p3/2 = 75.1 eV) and Au foil (Au 4f7/2 = 83.96 eV). Peaks were charged and referenced to the CHx band in the carbon 1-s spectra at 284.8 eV. Measurements were made at a take-off angle of 45° regarding the sample surface plane. This resulted in a typical sampling depth of 3-6 nm (95% of the signal originated from this depth or shallower). Quantification was accomplished using instrumental relative sensitivity factors that accounted for the x-ray cross-section and inelastic mean free path of the electrons. Major elements (>5 atom%) tended to have standard deviations of <3% on homogeneous samples, while minor elements could be significantly higher. The analysis size was \sim 200 µm in diameter. As shown in Fig. 3, the UV film contained C-O, C=O, and COO. Sample L20 contained fluorocarbons, CHx, organosilicon, SiO2, and protonated amines. Sample L35 contained fluorocarbons, CHx, protonated amines, COO (an ester), and sulphates. The anti-condensation coatings contained C-O and SiO₂.

2.2.1. Thermal conductivity

Based on the measured data, to calculate the overall heat transfer of the sample when condensation occurred, the thermal conductivity values of the samples needed to be acquired. To do this, a thermal conductivity measurement was performed using the Hot Disk TPS 3500 with a Kapton-insulated sensor (0.005–1800 W m⁻¹K⁻¹, -238 °C–400 °C). As shown in Fig. 4, these specimens (i.e., clear glass) were placed between two thermal blocks, while the Kapton sensor was clamped under the glass sample and sandwiched in by the specimens and one thermal block. The thermal properties were then calculated from the specimens' temperature changes resulting from the sensor's heat generation (Maeda, Tsunetsugu, Miyamoto, & Shibusawa, 2021; Ranjbarzadeh, Moradikazerouni, Bakhtiari, Asadi, & Afrand, 2019). The temperature rise across the sample depended on the thermal conductivity and thickness.

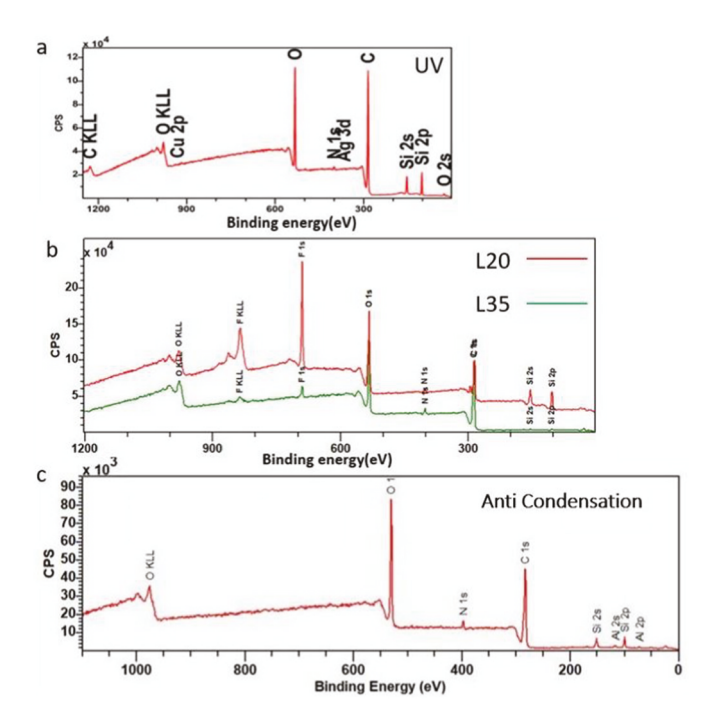


Fig. 3. (a) UV, (b) L20 and L35, and (c) anti-condensation chemicals on clear glass.

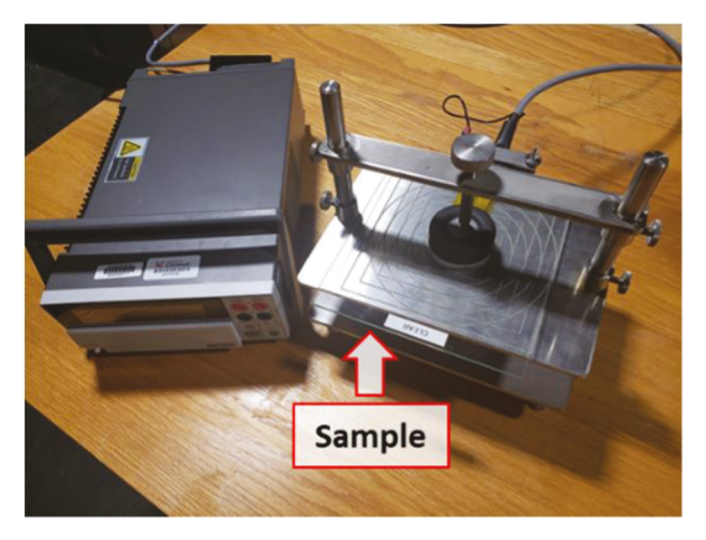


Fig. 4. Thermal conductivity measurements.

2.2.2. Emissivity

As mentioned above, surface emissivity can influence the overall heat transfer, condensate film formation, and associated condensation heat transfer coefficient. A standard emissivity measurement was performed using a portable emissometer (AE1 RD1). This required that the two samples be maintained at the same temperature. A heat sink provided with the equipment performed this function for the small flat samples mounted alongside the standard, as shown in Fig. 5. The detector was mounted on an aluminium heat sink that was electrically heated to a constant 71 °C. That sample (10 cm \times 15 cm) was placed on the heat sink, which maintained both the standard and sample at a temperature that was near ambient. Because there was a radiation heat input into the sample, the temperature at the surface began to rise immediately when the detector was moved into place. The temperature rises across the sample depended upon the thermal conductivity and thickness of the sample. The accuracy of the emissometer depended

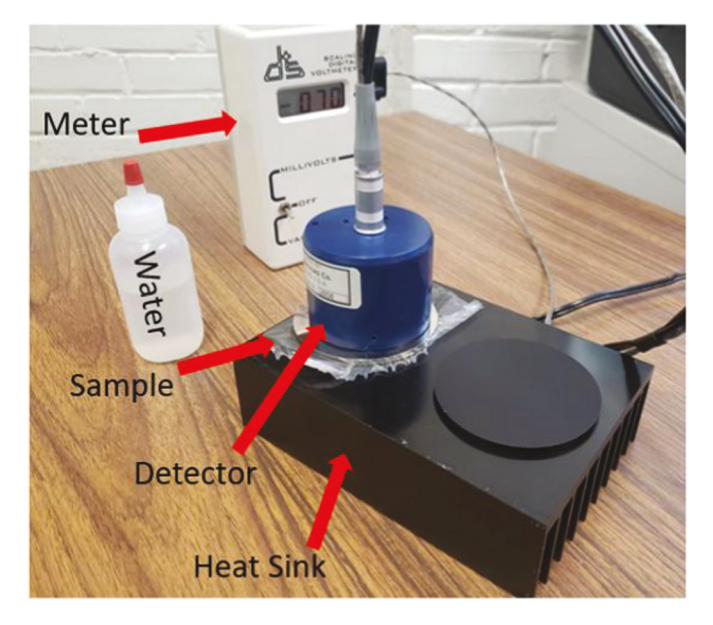


Fig. 5. Experimental setup of the emissivity measurement.

primarily on the linearity of the output voltage with emissivity and the accuracy of the standards used when taking the measurements.

2.2.3. Wettability measures

The wettability of a material's surfaces may affect the condensate surface film thickness, further influencing the overall heat transfer. In this work, the contact angle measurements were performed on a Rame-Hart goniometer model 590. A video camera was calibrated using a 4 mm ball bearing. Fresh DI water was used for all measurements, with a tested surface tension of 72 dyne/cm. The sample was levelled by adjusting the four-axis stage. The contact angle was measured in three locations on each sample. As can be seen in Fig. 6, both films resisted water droplets. The contact angle of L20 was 101°, L35 was 104°, UV was 75° , and clear glass was 51° . The water contact angle for L35 was slightly larger, due to the presence of COO (an ester) and sulphates that resisted the water (see Fig. 6), improving the water resistance property of the films. This project used an anti-condensation spray (SunClear) on the surface of the films and dried them. After adding the spray, the water contact angle of all films slightly increased, from 51° to 65° for clear glass, from 75° to 79° for UV, from 101° to 105° for L20, and from 104° to 109° for L35.

2.3. Filmwise condensation heat transfer coefficient calculation from measured data

In a two-dimensional steady-state heat transfer situation, the

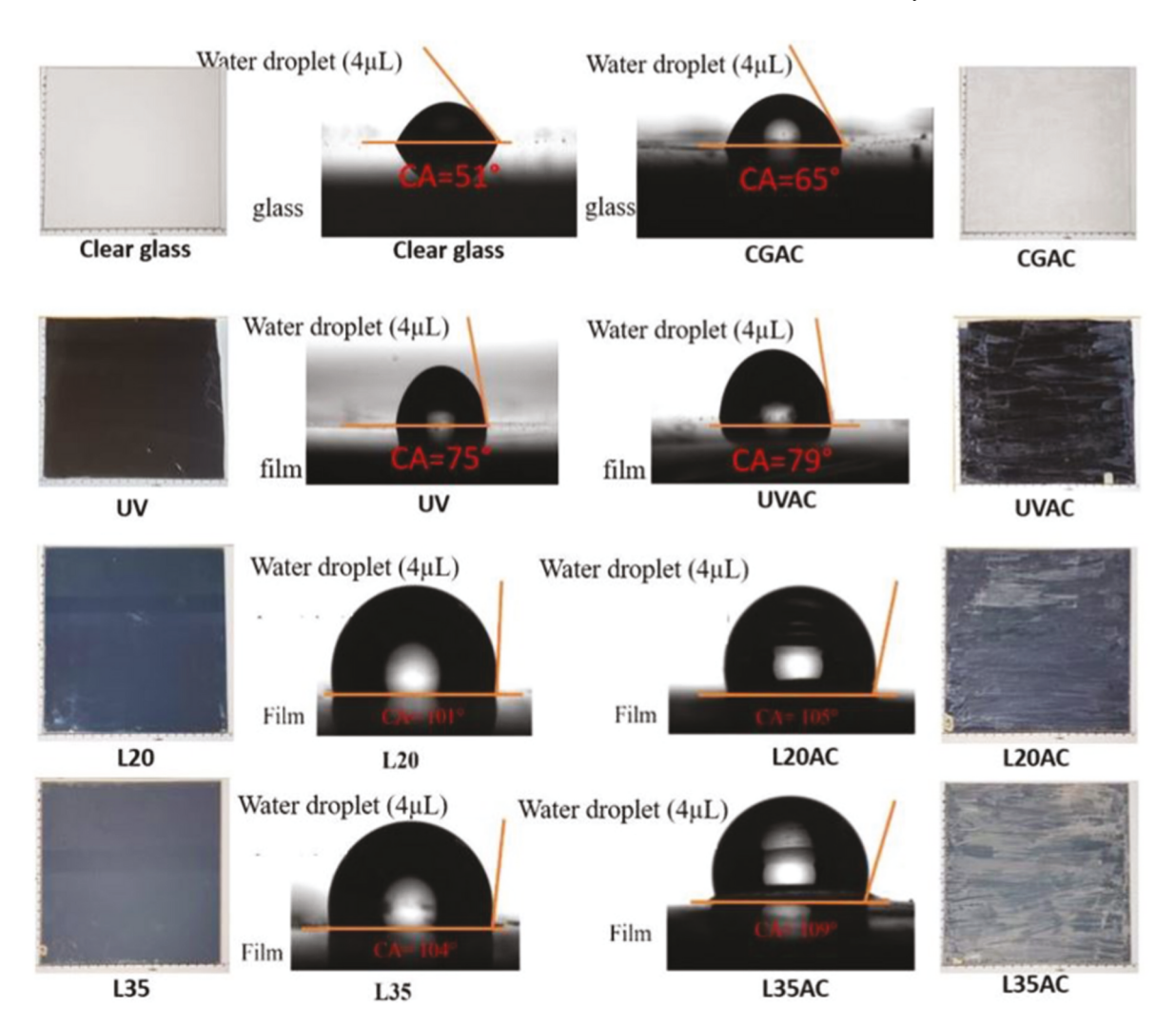


Fig. 6. Specimens and contact angles.

following relationship between the overall heat transfer and heat transfer coefficient for each layer can be obtained, as shown in Equation (1). Notably, like the surface film coefficient used in the American Society of Heating and Air-Conditioning Engineers handbook (ASHRAE), the surface film heat transfer coefficient represents the combination of both radiative and convective heat transfer (ASHRAE, 2013).

$$Q_{total} = U_{total} * A * (T_i - T_o) = h_c * A * (T_i - T_{gi}) = \frac{1}{R_{specimen}} * A * (T_{gi} - T_{go})$$
(1)

where $Q_{tol,e}$ in unit W is the overall heat transfer (as measured by the heat flux sensor in the experiments), U_{total} in unit $W \cdot m^{-2} K^{-1}$ is the overall heat transfer coefficient (U-factor), $R_{specimen}$ in unit $m^2 \ K \cdot W^{-1}$ is the specimen's R-value used in the experiment and measured via the Hot Disk TPS 3500, h_c in unit $W \cdot m^{-2} K^{-1}$ represents the condensation heat transfer coefficient, T_o in unit °C is the ambient temperature in the chamber, T_i , °C is the inner-space temperature of the psychical box, T_{gi} , °C is the specimen's inner surface temperature, T_{go} , °C is the outer surface temperature, and A is the surface area (in m^2) of the test box opening. These parameters are also shown in Fig. 7. $h_{c,e} * A * (T_i - T_{gi})$ is the heat flux calculation for the water condensate layer. The condensation heat transfer coefficient from experiment $h_{c,e}$, $W \cdot m^{-2} K^{-1}$ (in which the subscript e denotes that this is obtained based on the experimental data) can be inferred via Equation (2) by using overall heat transfer $Q_{tol,e}$, W and other parameters measured in experiments.

$$\frac{1}{h_{c,e}} = \frac{\left(T_i - T_{go}\right)}{Q_{tol,e}} - R_{specimen} \tag{2}$$

2.4. Filmwise condensation heat transfer coefficient calculation from theoretical models

Water condensation on glazing surfaces occurs in two main modes: filmwise and dropwise. Filmwise condensation results in a thin, continuous liquid film that wets the surface, while dropwise condensation occurs as discrete liquid droplets. Several factors, including the outdoor temperature, glazing insulation, internal glass surface temperature, and indoor relative humidity, influence water condensate formation on a glazing system's interior surface (Duan, Q., Zhao, Y., & Wang, J. (2020). When the surface temperature of the glass equals or falls below the dew point temperature, water condensate forms on the glass surface. Both types of condensation can occur simultaneously, with filmwise condensation representing the final stage and dropwise condensation representing the transition state. The liquid film in filmwise condensation carries the heat transfer rate and thermal resistance of the condensate.

Filmwise condensation is dominant in tremendous applications, such as HVAC systems, electronic devices, solar stills, and building window systems. Studies on filmwise condensation are prevalent in the literature, with many investigating its effects on heat transfer and thermal insulation. For example, Feuilloley and Issanchou (1996) used a hot box method and mass transfer of water to study the effects of condensation on glass and plastic, finding an increased heat loss on glass from condensation, Bhardwaj, ten Kortenaar, and Mudde (2013) studied the influence of the condensation surface in a solar distillation system and found that the condensation model did not significantly affect overall heat transfer. However, other studies have shown that condensation on a glazing system can damage its overall insulation ability. For example, Eimann et al. (2018) investigated the heat transfer coefficients of dropwise condensation in a horizontal channel and proposed a new correlation function based on the Reynolds number. They concluded that dropwise condensation on a vertical wall can be treated as filmwise condensation.

There are two models used to calculate the filmwise condensation heat transfer coefficient. One is the one-film condensation model and the other is the double-film model. Nusselt's filmwise condensation theory (with one film) has proven successful for pure vapour situations in the absence of condensate film, inertia, and convection terms (Chen, 1961; Koh, Sparrow, & Hartnett, 1961; Kulacki et al., 2018; Nusselt, 1916; Sparrow & Gregg, 1959). The double-film model was established based on the work by Sparrow in 1967 and Rose in 1980, in an effort to consider dry air and the air vapour layer formed outside the condensate water film (Rose, 1980; Sparrow, Minkowycz, & Saddy, 1967). Both models are shown below in Fig. 7. The most significant difference is that the double-film model involves two interfacial parameters: the mass fraction of the non-condensable gas and the interface temperature T_r , °C (Duan, Hinkle, Wang, Zhang, & Memari, 2021).

 T_r is the reference temperature between the two layers, condensate water film, and dry air film (as shown in Fig. 7). It is not measurable but can be calculated based on numerical analysis of the conventional Nusselt model and heat transfer in the presence of dry air (Minkowycz & Sparrow, 1966). Poots validated Voskresebskiy's theory and yielded a -3.3% error. He evaluated the expression model at the reference temperatures for Nusselt, Rohsenow, and Chen and found the coefficient β table for T_r calculation, as listed (Poots & Miles, 1967). T_r is calculated based on the heat transfer of dry air and the conventional Nusselt model, and the use of coefficient β .

According to the conventional one-film Nusselt model, the conventional heat transfer coefficient h_c , W·m⁻²K⁻¹ for the condensate water film on the L length of a vertical surface is expressed as in Equation (3):

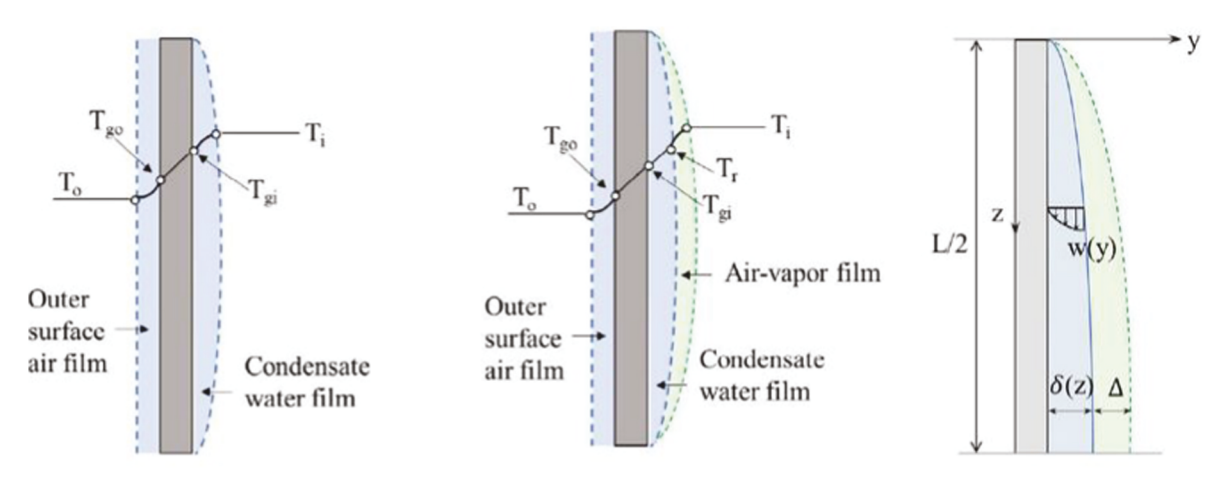


Fig. 7. Thermodynamic schematics of filmwise condensation (Duan et al., 2021).

$$h_c = 0.943 \left[\frac{\Delta H_v \rho(\rho - \rho_v) g k^3}{4\mu (T_r - T_{gi}) L} \right]^{\frac{1}{4}}$$
 (3)

Where k in unit W·m⁻² K⁻¹ is the thermal conductivity, L in metre is the z-dimensional length of the film condensed on the vertical surface, ΔH_{ν} in unit kJ·kg⁻¹ is the latent heat of evaporation, ρ in unit kg·m⁻³ is the density of the liquid, ρ_{ν} in unit kg·m⁻³ is the density of the vapour, g in unit m³·kg⁻¹s⁻² is the gravitational constant, and μ in unit kg·m⁻¹s⁻¹ is the dynamic viscosity.

$$T_r = T_{gi} + \beta (T_i - T_{gi}) \tag{4}$$

Where T_i , °C is the inner space temperature of the psychical box and T_{gi} , °C is the specimen's inner surface temperature. $\beta = \beta_0 + \beta_1 * \left(\frac{\Delta T}{T_{gi}}\right) + \beta_0 * \left(\frac{\Delta T}$

$$\beta_2 * \left(\frac{\Delta T}{T_{gl}}\right)^2$$
, where β_0 , β_1 , and β_2 are the values listed in Table 2.

The condensation heat transfer coefficient $h_{c,doub}$, W·m⁻²K⁻¹ (in which subscript refers to the value being obtained based on the double film theory) is shown below.

$$h_r = \frac{h_c (T_r - T_{gi})}{(T_i - T_{gi})} \tag{5}$$

$$h_{c,doub} = \frac{1}{\frac{1}{L} + \frac{1}{L}} \tag{6}$$

Ultimately, Equation (7) is used to calculate the overall centre-of-specimen U-factor, U_{total} , W·m⁻²K⁻¹, the h_c value is used according to the condition with condensation.

$$U_{total} = \frac{1}{R_{specimen} + R_{air} + \frac{1}{h_{c}}} \tag{7}$$

3. Results

3.1. Material properties

This process used the properties (see Table 3) of each specimen obtained through material characterisation (see Section 2.2). In general, these three material or surface properties were aligned with the expectations of experimental design. The coatings or additives on the clear glass surface generally altered the thermal transfer coefficient. The thermal conductivity was measured for the clear glass in Section 2.3.1; the value was 0.194 W m⁻¹K⁻¹ for an 8 mm thickness. This gave the thermal resistance value $R_{specimen}$ of 0.04 m²K·W⁻¹. The conductivity levels of the other specimens were also evaluated and converted to the R-values listed in Table 3. With the addition of layers of materials, the insulation of the specimen increased slightly, but the overall insulating ability of all samples was still quite low (for instance, the insulation of a typical dry-air surface film is about 8.48 W m⁻²K⁻¹ for a clear glass, based on ASHRAE, 2013 and shown in Section 3.3.1).

In addition to the insulation features of the specimens, Table 3 shows that the adding of Low-E coatings effectively reduced the emissivity values of the samples, while the additional anti-condensation chemicals slightly increased the surface emissivity of the Low-E surfaces. Also, it was consistent that the anti-condensation additives slightly increased the contact angle of the original surface, due to their hydrophobic properties. Fig. 8 also shows a general negative relationship between the

Table 2Estimates of coefficients (Poots & Miles, 1967).

	eta_0	eta_1	β_2
Nusselt	0.2474	0.1580	-0.0769
Rohsenow	0.1602	0.1649	-0.0356
Chen	0.2228	0.1003	-0.0255

Table 3Key material properties of each specimen.

SN Sample	Samples	Samples Thermal Conductivity	R _{specimen}	Emissivity (Coating Surface)	Contact Angle
		$W \cdot m^{-1} K^{-1}$	$m^2 K \cdot W^{-1}$	_	0
1	Clear glass	0.194	0.041	0.933	51
2	CGAC	0.178	0.045	0.892	65
3	UV	0.084	0.095	0.896	75
4	UVAC	0.087	0.092	0.890	79
5	L20	0.110	0.072	0.428	101
6	L20AC	0.107	0.075	0.700	105
7	L35	0.125	0.064	0.637	104
8	L35AC	0.139	0.058	0.840	109

contact angle and emissivity (Trosseille et al., 2022). From left to right, the contact angle increased while the emissivity decreased in response to different coatings and/or surface treatments. This was mainly because this experiment's key elements used for low emissivity also exhibited certain hydrophobic features. In particular, the UV film contained Ag and Cu particles, while the L20 and L35 coatings contained fluorocarbons and an infrared reflective layer of metallic elements. These elements made the surfaces exhibit low emissivity (and durability) features (Dong et al., 2022; Wang et al., 2011). In addition, the homogeneous C-O bond found in the anti-condensation and UV film could also control infrared radiation properties via its vibration range (i.e., the C-O bond length), reducing infrared emissivity (Zhu et al., 2021). In terms of the contact angle, more metallic particles on the specimen's surface also caused an increased contact angle (FOWKES, 1964; Murono, Takahiro, Kenta Hongo, & Maezono., 2022), and fluorocarbon-based surfaces are typically hydrophobic because of their low surface energy and great molecular cross-sectional area (Dalvi & Rossky, 2010; Lemal, 2004).

3.2. Condensation effects model for heat transfer and validation

In Section 2.5, this paper discussed two analytical models that can be used to calculate the condensation heat transfer coefficient. To obtain such value for the one- and double-film models, we used Equations (1) and (4), respectively. A comparative analysis then was conducted using experimental data for a clear glass specimen, in which the accuracy of the one- and double-film models and the expression model at reference temperatures were examined and compared. The results of the comparison are presented in Fig. 9. The findings indicate that the one-film approach based on the conventional Nusselt model h_c yielded a averaged value that was 31.9% higher than the one calculated ($h_{c.expr}$) based on the experimental data. In contrast, the double-film model $h_{c.doub}$ developed in Section 2.5 showed mean error rates of 3.6%, 39.5%, and 28.5% with the model expressions of Rohsenow, Nusselt, and Chen, respectively. The analysis determined that the double-film model with Rohsenow's expression was the most accurate. It is worth noting that this conclusion was based on filmwise condensation in typical greenhouse glazing materials and a greenhouse indoor environment characterised by a temperature of 25 °C and RH of 60% in an ambient winter temperature of 0 °C.

The condensation heat transfer coefficient calculated based on the experimental data across all specimens was used to validate the double-film model further. The validation results are shown in Fig. 10 and consist of two sets of condensation heat transfer coefficients generated from the experiments and simulated via the established double-film model. The figure shows that the proposed analytical model was in good agreement with the experimental data (4.42% mean relative error). This confirmed the applicability of the theoretical double-film model for the greenhouse condensation heat transfer coefficient analysis.

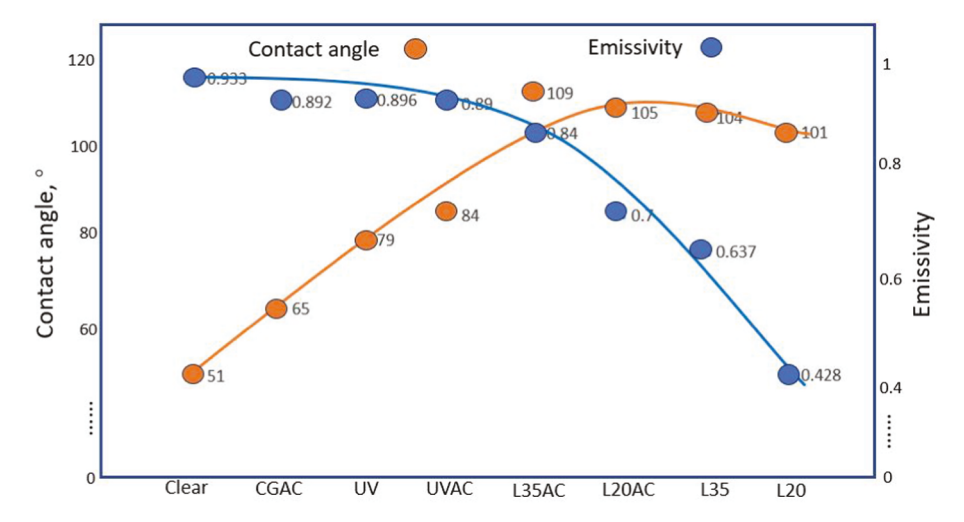


Fig. 8. Contact angle and emissivity.

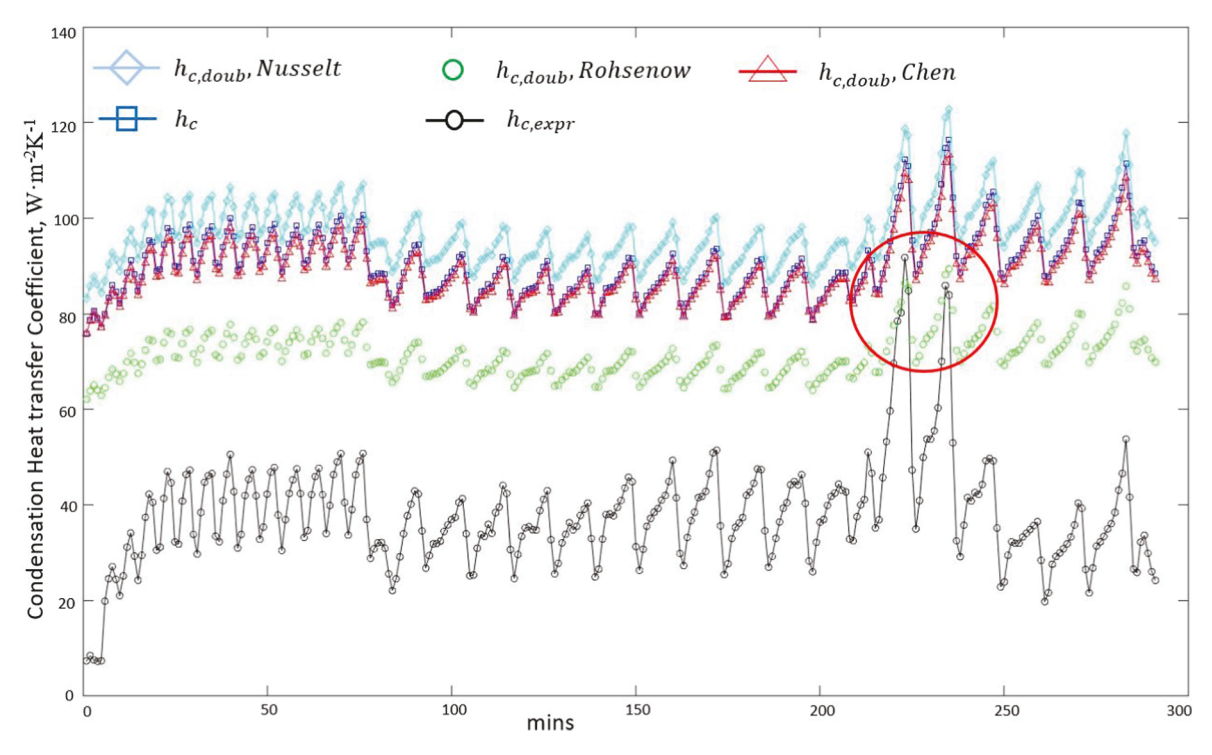


Fig. 9. Experimental model validation for the clear glass.

3.3. Condensation's effects on the overall heat transfer coefficient (Ufactor)

3.3.1. Condensation heat transfer coefficient variations

According to the ASHRAE, 2013 handbook, the surface film heat transfer coefficient combines radiative and convective heat transfer that depend on surface emissivity and film humidity conditions, respectively (ASHRAE, 2013). In the U-factor calculation for the greenhouse (or general building) coverings, the surface film heat transfer coefficient plays an essential role, especially with regard to inadequate insulation. For instance, for a three mm-thick single-pane glazing, the insulating ability of the inner surface film is about forty times higher than glass insulation if the inner surface film is in dry air conditions.

It was anticipated that the condensation effect would significantly impact the surface film heat transfer coefficient in this study. When condensation occurs, a condensate film replaces the surface film, which

combines dry air, vapour, and liquid. This increases surface emissivity and moisture content, leading to an enhanced heat transfer coefficient. This value for the inner surface was obtained using experimental measurements and calculated using Equations (5) and (6). Table 4 demonstrates a substantial difference between the coefficient values before and after condensation conditions. For example, the heat transfer coefficient increased from 8.48 to 91.7 W $m^{-2}K^{-1}$ for clear glass. In other words, the original insulating ability of the dry-air-dominated surface film was entirely diminished due to the condensation effect. This effect was more prominent in cases where the original surface film coefficient was lower and without condensation effects, such as the specimen with Low-E coated glazing which increased over eleven times from 5.54 to 63.6 W $m^{-2}K^{-1}$. The glazing applied with anti-condensation coatings exhibits overall better thermal performance when condensate because of its capability to absorb water and limit the effect of condensation.

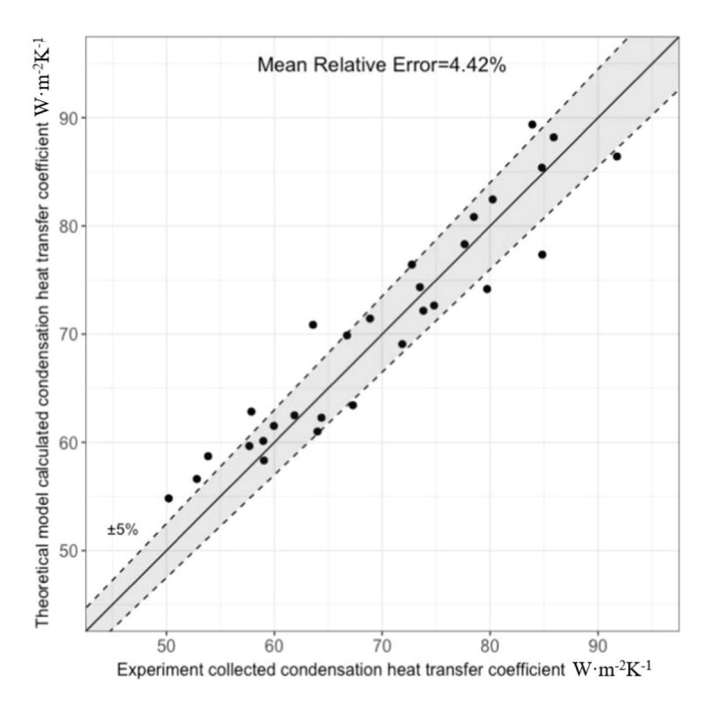


Fig. 10. Validation of the double-film model for all specimens.

Table 4Surface film heat transfer coefficient with and without condensation.

SN	Samples	Without condensation	With condensation	Increasing rate
		$W \cdot m^{-2} K^{-1}$	$W \cdot m^{-2} K^{-1}$	%
1	Clear glass	8.48	91.7	1080
2	CGAC	8.24	84.8	1030
3	UV	8.26	79.2	958
4	UVAC	8.23	73.8	896
5	L20	5.54	63.6	1150
6	L20AC	7.12	59.0	827
7	L35	6.76	67.3	995
8	L35AC	7.94	64.4	810

3.3.2. Overall heat transfer coefficient (U-factor) variations

The original U-factor of the specimens was simulated by taking the heat transfer coefficients (for both the inner and outer surfaces) and the glazing layer's thermal properties into account. The simulation was using the WINDOW 7.8 software developed by the Lawrence Berkeley National Laboratory (Curcija et al., 2015). Clear float glass (ID 8203) was used as the baseline reference (with single pane glazing and without any coatings/films), as well as 3M L20 (ID 2793), 3M L35 (ID 2714), and UV block film (ID 27801). Notably, the substrate type (i.e., single-pane clear glass) and exterior surface film heat transfer coefficient were the same across all simulations. Thus, the only cause for U-factor variation was the interior surface film heat transfer coefficient. The standardised conditions defined by the National Fenestration Rating Council (NFRC) for computing the U-factor were adopted in this calculation, which is

Table 5
Standardised conditions for winter U-factor calculations.

Name	Inside	Outside	Unit
Air Temperature Convection Coefficient Air Velocity Effective Room Temperature Direct Solar Radiation	21.0 6.980 0.00 21.0	-18.0 26.000 5.50 -18.0	$^{\circ}$ C W·m ⁻² K ⁻¹ m·s ⁻¹ $^{\circ}$ C W·m ⁻²
Effective Room Emissivity	1.0	1.0	

Table 6U-factor with and without condensation conditions.

SN	Samples	Without condensation	With condensation	Increasing rate
		$W \cdot m^{-2} K^{-1}$	$W \cdot m^{-2} K^{-1}$	%
1	Clear glass	5.89	15.94	170.6
2	CGAC	5.76	15.62	171.1
3	UV	3.78	6.41	69.5
4	UVAC	3.83	6.52	70.4
5	L20	4.51	17.59	289.8
6	L20AC	4.45	9.89	122.1
7	L35	4.82	13.43	178.8
8	L35AC	4.98	11.06	122.2

shown in Table 5. Such standards are also applied to the transparent coverage systems used in greenhouse facilities.

The U-factors for two conditions, with and without condensation, are also presented later in Table 6 and Fig. 11, where the U-factor with condensation effect was calculated using Equation (7) in section 2.5. The U-factor increased enormously, ranging from 69.5% to 298.8%, depending on the surface type. Again, the condensation's effects on the U-factor of the Low-E coated glazing are relatively more significant, with almost a three-fold increase in U-factor from 4.51 to 17.59. In contrast, other samples such as the UV film only increased about 70 percent on its U-factor with the condensation effect. Such performance of UV products may benefit from its low value of the contact angle and its originally strong insulation.

3.3.3. Effect of surface properties on the condensation heat transfer coefficient

As mentioned in the introduction, surface wettability theoretically determines the eventual influence of the condensate film. After inputting the experimental data collected during the filmwise condensation stage into Equation 3 through 6, the condensation heat transfer coefficient $h_{c,doub}$ was determined. The results for each specimen and corresponding contact angle (CA) were then also analysed.

$$h_{c,doub} = \sqrt{-79.7 * CA + 12396.8} \tag{8}$$

The study results showed a clear negative correlation between the contact angle and the filmwise condensation heat transfer coefficient, as depicted in Fig. 12, a. This suggests that as the contact angle increases, a larger region exists between the liquid-vapour and solid surfaces, leading to condensate films having more vapour-air mixture and mitigating the overall film heat transfer. Although the data sample in this study was limited, the relationship (Equation (8) with an R-squared of 0.952) between the contact angle and condensation heat transfer was evident. Such relationships can quickly estimate the condensation effects on overall heat transfer for the greenhouse facilities.

On the other hand, when considering emissivity as shown in Fig. 12, b, there is no clear relationship between emissivity and condensation heat transfer coefficient. As if it includes emissivity as a factor in Equation (8), the $\rm R^2$ went down to 0.943 from 0.952. Both evidence indicated that emissivity at condensation conditions has no significant effect on condensation heat transfer coefficient prediction.

4. Discussion

4.1. Physical basis of condensation impacting insulation

Water condensation on these surfaces engenders a notable attenuation in their capacity for thermal insulation as shown in Fig. 11, which may be attributed to two core factors. Primarily, the emissivity of the inner surface experiences elevation due to the presence of condensed water, a consequence of water's comparatively higher emissivity when juxtaposed with the majority of coated glazing surfaces. This adjustment

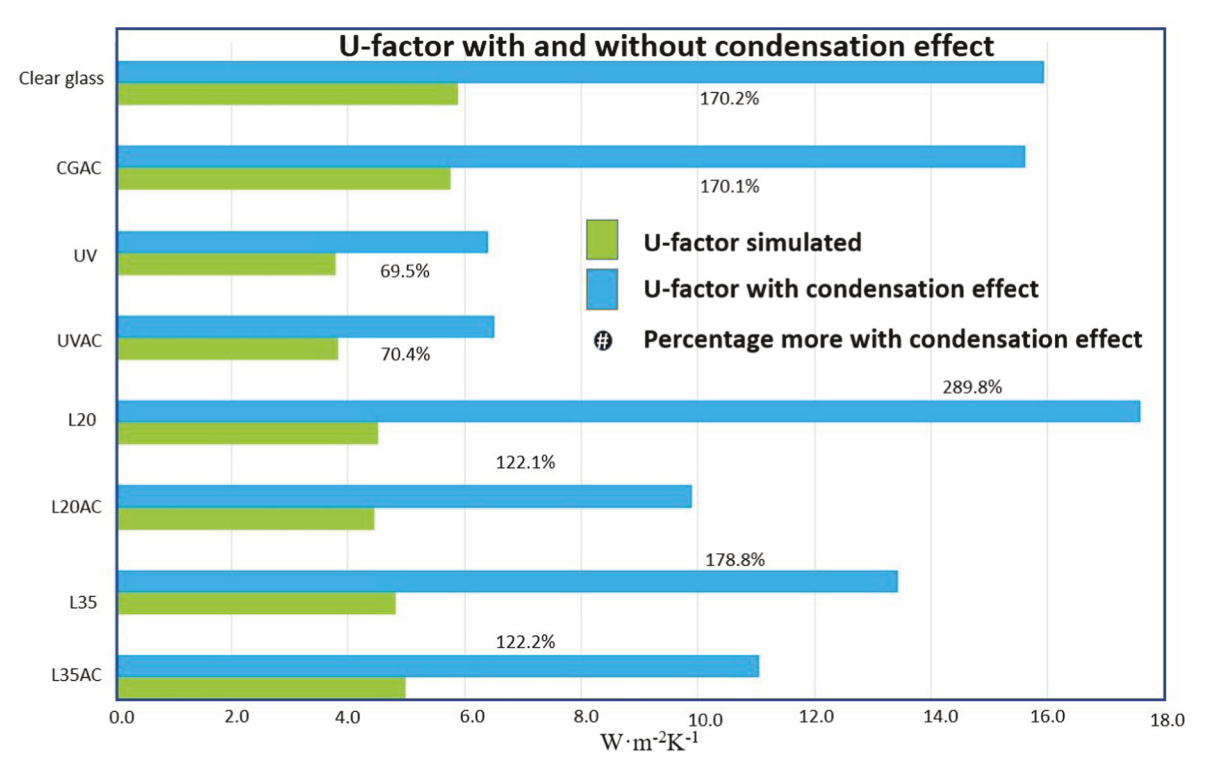


Fig. 11. U-factor with and without condensation.

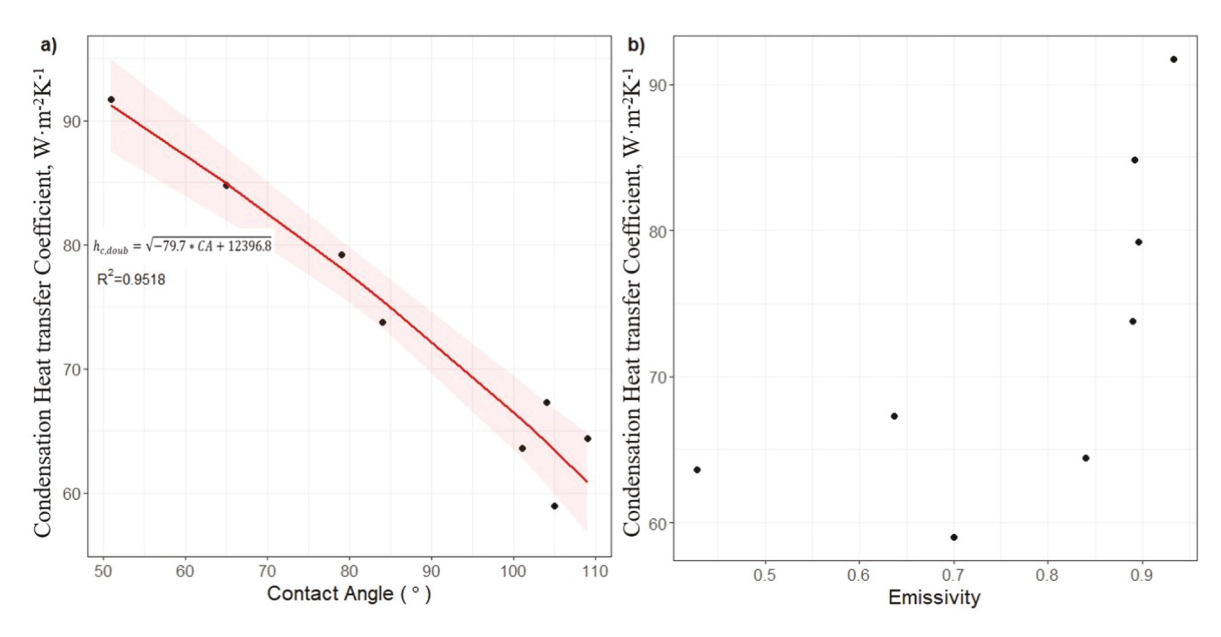


Fig. 12. Contact angle's effect on the condensation heat transfer coefficient, (left)contact angle vs. condensation heat transfer coefficient; (right) emissivity vs. condensation heat transfer coefficient.

results in an augmented radiative heat transfer process. Furthermore, the water content ensconced within the surface film serves to accentuate convective heat transfer between the ambient conditions within the greenhouse's interior and the inner surface. This development transpires due to the establishment of a fresh condensation film, encompassing liquid, vapour, and dry air components, effectively supplanting the original surface film, hitherto solely governed by dry air-mediated dynamics (Duan et al., 2021). Additionally, in this study, single-pane glazing was assumed. Another major type of the greenhouse covering materials is thin plastic, which may have even lower insulation abilities than glass. Accordingly, it can be expected that there will be a greater

change in the U-factor of plastic greenhouse coverings if condensation occurs.

The results indicated some potential issues if Low-E and IR products are recommended for energy-saving purposes in greenhouse facilities. Although a variety of Low-E products and retrofit methods, such as adhesive films and sprayable additives, have been widely accepted as important energy-saving strategies, the evidence obtained in this work shows that they may lead to adverse effects on the operational energy use when the condensation effect is taken into account. Combined with the increased condensation risks of Low-E surfaces (due to the lower surface temperature as compared to high emissivity surfaces),

conditions in the winter season may significantly increase the condensation risk associated with adding Low-E features to greenhouses. Even though certain uses in greenhouses may save energy because of the increased insulation that Low-E products provide, the dramatically increased energy loss caused by the condensation effect may easily offset such benefits.

4.2. Trade-off of using Low-E features in the greenhouse covering materials

The results in section 3.3.3 indicated a negative relationship between the contact angle and the condensation heat transfer coefficient, which was expressed as a regression model. In other words, as the contact angle gets larger, the insulation of filmwise condensation becomes smaller, which eventually results in a large U-factor increase (for example Low-e surface). Assuming that the filmwise condensation was uniformly formed, and as shown in Fig. 6 an increased contact angle of a surface formed a bigger (thicker) condensate droplet, which could also indicate a thicker condensation film. Thus, the growth of condensation resulted in the expansion of the U-factor. That meant a filmwise condensation rather caused large heat loss because of the low thermal conductivity of the water than enhanced thermal insulation as many people claimed (Ho & Leong, 2021; Oh et al., 2018). On the other hand, the results indicated that the condensation heat transfer coefficient was not significantly correlated with base surface emissivity, as shown in Fig. 12. This can be explained by the fact that the condensate film had already fully covered the entire base surface, so only the water emissivity was involved in the surface heat exchange. In other words, once the condensation effect occurred on the greenhouse's inner surface, the original base surface emissivity became irrelevant to the overall thermal performance of the coverage system. Such a result is similar to Troseille et al. (2022) when they concluded that water eventually becomes the dominant contributor to the substrate's effective emissivity in their experiment of testing wet substrate.

Alongside the previous discussions, although Low-E and IR reflective features are proven to enhance the energy savings of the greenhouse operationally, the frequent presence of condensation phenomenon still could eliminate the insulation and cause huge heat loss. Therefore, there was a trade-off between the energy savings from Low-E features and the energy lost due to the increased condensation risks caused by Low-E. As Duan et al. (2021) pointed out, the envelope's inner surface condensation occurs more often in cold and humid climates or weather conditions, with envelopes having low thermal insulating abilities. However, when condensation does not occur in warm climates or seasons, the significant energy-saving goal of using Low-E and IR additives can still be achieved. To make optimal selections, more comprehensive whole-year energy simulations taking the condensation effect into consideration, followed by comprehensive energy performance analyses and comparisons, are needed. To conduct such analyses, the dynamic condensation-driven U-factor (Eq. (7)) needs to be integrated into the simulation procedure, which can be done by parametric energy simulation methods linking surface temperature and indoor temperature and humidity in the simulation tool (Wang & Beltran, 2016).

4.3. Potential improvement or treatments

In theory, the condensation phenomenon can be prevented or mitigated when it comes to the situations - either the surface temperature is higher than the dew point temperature of the indoor air or the RH of indoor air is at a lower band. However, the RH in a greenhouse environment is normally maintained at a high level for plant growth purposes. Therefore, the possible strategies should focus on increasing surface temperature, which could be related to the following pathways.

First, strong insulation of the covering materials could usually lead to a high surface temperature, such as double pane glazing or double layer plastics, which can use the air gap layer to reduce heat loss and increase

the surface temperature of the inner surface even in a low-temperature outdoor condition (Maraveas, 2019; Zhang, Jahid, & Wang., 2023). Yilmaz and Çetintaş (2005) proposed a new modification method and concluded an average 4 °C higher inner surface temperature of double pane glass than single ones for the south façade in Istanbul. Such founding, understanding, and method could be used in the study of various covering materials in greenhouse and horticulture coverings, including glasses and plastics. Second, the phenomenon of metallic nanoparticles' spectral-selective and photothermal effects has been well studied (Wang & Shi, 2017), which can be also integrated into the design of the surfaces of the greenhouse covering materials for daytime condensation situations. Zhang, Duan, Wang, Zhao, and Feng (2021) developed a mathematical expression of Fe₃O₄@Cu_{2-x}S with a strong photothermal effect. The model successfully predicted its surface temperature increase under 1000 W·m⁻² illumination power and such a phenomenon brought a much higher surface temperature than the conventional heat transfer model prediction under such a lighting condition. The nanoparticles were coated on a glass surface, and more substrates can be developed in the future. Third, as the lowest inner surface temperature may always happen during the nighttime of the greenhouse operation, direct solar radiation is absent. Phase change materials (PCM) as an alternative can store daytime solar energy and release the heat till nighttime. Xie, Wang, Sang, and Liu (2018) examined a graphite-modified PCM and found that after approximately 2 h under a solar simulator, such material can release heat for about 4 h at room temperature range. The surface temperature difference of this PCM can be up to 1.0 °C higher than the gypsum component. Although the release hours are shorter than usual 6-8 h of nighttime, this paves a new way for using PCM at room temperature. Other methods, such as geothermal heating systems and waste heat collection systems are widely used and discussed in residential, commercial buildings, and agriculture facilities (Ahamed et al., 2019; Lund & Toth, 2021). The way they are used to heat indoor space by collecting the available heat source could also enhance the surface heating of the greenhouse coverings. Those opportunities and applications discussed above in the greenhouse could be investigated further for the prevention of the condensation effect.

5. Conclusion

This study investigated the relationship between surface properties and U-factor during condensation, specifically surface emissivity, and wettability (measured by contact angle). The experimental and computational results demonstrate that contact angle plays a critical role in determining the filmwise condensation thickness on a surface, dramatically impacting the U-factor. We found that surfaces with higher contact angles, such as those treated with IR-reflective additives and Low-E coated glass, can have significantly reduced insulation during water condensate conditions, particularly in winter. On the other hand, surface emissivity, which is an essential factor in determining the surface film coefficient, did not significantly impact the U-factor while water condensed.

Furthermore, this study quantitatively validated a simplified double-film model previously proposed in the literature. The results confirm that this model offers better accuracy than a one-film model for clear glass in typical indoor environments at a temperature of $25\,^{\circ}\text{C}$ and RH of 60% in winter, with an ambient temperature of 0 $^{\circ}\text{C}$. We also extended and evaluated the model for other representative surfaces, including UV, Low-E, and anti-condensation additives. This validated double-film model can now be used in computational analysis for predicting overall energy performance in greenhouse facilities.

In addition, this work developed a regression function to correlate contact angle and condensation heat transfer coefficient, revealing that a higher contact angle reduces the coefficient of filmwise condensation. This relationship can be useful for rapidly analysing and estimating the effects of condensation on the U-factor and can help with decision-

making regarding material and additive selections for greenhouse facilities. This work is the first to systematically investigate the role of contact angle and emissivity in the overall condensation heat transfer.

One aspect of this study that invites further exploration is the examination of a single representative condensation scenario (filmwise condensation across the entire surface, attributable to the size of the glazing sample used in the experiments). In practical scenarios, it's common to observe another form of condensation, which primarily occurs at the perimeter areas of the surface. In these instances, the original material's surface emissivity might still influence the U-factor, especially if the condensate water film doesn't entirely envelop the base surface. Such scenarios are frequently encountered in real-world greenhouse conditions, attributable to non-uniform thermal distribution on the surface and/or localised heating conditions. In these cases, the U-factor should be assessed using an area-weighted method, accounting for condensate and non-condensate surface characteristics. The double-film theory and parameters validated in this study can also be applied to the condensate section. These aspects offer promising directions for future investigation.

CRediT authorship contribution statement

Enhe Zhang: Investigation, Writing - original draft, Data curation, Formal analysis, Validation. Md Anwar Jahid: Materials measurements and Characterisation. Julian Wang: Conceptualisation, Methodology, Funding acquisition, Writing - review & editing, and Project administration. Nan Wang: Data modelling and Visualisation. Qiuhua Duan: Experiments and Theoretical models.

Declaration of competing interest

The authors declare that they have no known competing financial interests or personal relationships that could have appeared to influence the work reported in this paper.

Acknowledgments

We acknowledge the financial support provided by the USDA Natural Resources Conservation Service NR203A750008G006 and National Science Foundation CMMI-2001207 and 1953004.

References

- Agrebi, S., Chargui, R., Tashtoush, B., & Guizani, A. A. (2021). Comparative performance analysis of a solar assisted heat pump for greenhouse heating in Tunisia. *International Journal of Refrigeration*, 131. https://doi.org/10.1016/j.ijrefrig.2021.06.004
- Ahamed, M. S., Guo, H., & Tanino, K. (2019). Energy saving techniques for reducing the heating cost of conventional greenhouses. *Biosystems Engineering*. https://doi.org/ 10.1016/j.biosystemseng.2018.10.017
- Al-Kayeim, H. H., Aurybi, M. A., & Gilani, S. I. U. (2019). Influence of canopy condensate film on the performance of solar chimney power plant. *Renewable Energy*, 136. https://doi.org/10.1016/j.renene.2019.01.067
- Amani, M., Foroushani, S., Sultan, M., & Bahrami, M. (2020). Comprehensive review on dehumidification strategies for agricultural greenhouse applications. Applied Thermal Engineering, 181. https://doi.org/10.1016/j.applthermaleng.2020.115979
- Asdrubali, F., & Baldinelli, G. (2011). Thermal transmittance measurements with the hot box method: Calibration, experimental procedures, and uncertainty analyses of three different approaches. *Energy and Buildings*, 43(7). https://doi.org/10.1016/j. enbuild.2011.03.005
- ASHRAE. (2013). 2013 ASHRAE handbook fundamentals (SI edition). 2013 ASHRAE Handbook—Fundamentals (IP). 2013(38).
- Bhardwaj, R., ten Kortenaar, M. V., & Mudde, R. F. (2013). Influence of condensation surface on solar distillation. *Desalination*, 326. https://doi.org/10.1016/j. desal.2013.07.006
- Chen, M. M. (1961). An analytical study of laminar film condensation: Part 1-Flat plates. Journal of Heat Transfer, 83(1). https://doi.org/10.1115/1.3680467
- Curcija, D. C., Zhu, L., Czarnecki, S., Mitchell, R. D., Kohler, C., Simon, V., et al. (2015).

 Berkelev. LAB WINDOW.
- Dalvi, V. H., & Rossky, P. J. (2010). Molecular origins of fluorocarbon hydrophobicity. Proceedings of the National Academy of Sciences of the United States of America, 107 (31). https://doi.org/10.1073/pnas.0915169107

- Dong, R., Du, T., Dong, S., Zhao, X., Ma, R., Du, A., et al. (2022). A weather-resistant daytime radiative cooler based on fluorocarbon resin. Solar Energy Materials and Solar Cells, 235. https://doi.org/10.1016/j.solmat.2021.111486
- Dragićević, S. M. (2011). Determining the optimum orientation of a greenhouse on the basis of the total solar radiation availability. *Thermal Science*, 15(1). https://doi.org/ 10.2298/TSCI100220057D
- Duan, Q., Hinkle, L., Wang, J., Zhang, E., & Memari, A. (2021). Condensation effects on energy performance of building window systems. *Energy Reports*, 7. https://doi.org/ 10.1016/j.egyr.2021.10.096
- Duan, Q., Zhao, Y., & Wang, J. (2020). Thermal performance and condensation risk of single-pane glazing with low emissivity coatings. MRS Advances, 5, 2555–2564.
- Eimann, F., Zheng, S., Philipp, C., Fieback, T., & Gross, U. (2018). Convective dropwise condensation out of humid air inside a horizontal channel – experimental investigation of the condensate heat transfer resistance. *International Journal of Heat* and Mass Transfer, 127. https://doi.org/10.1016/j.ijheatmasstransfer.2018.08.015
- Fabrizio, E. (2012). Energy reduction measures in agricultural greenhouses heating: Envelope, systems and solar energy collection. *Energy and Buildings*, 53. https://doi.org/10.1016/j.enbuild.2012.07.003
- Feuilloley, P., & Issanchou, G. (1996). Greenhouse covering materials measurement and modelling of thermal properties using the hot box method, and condensation effects. *Journal of Agricultural Engineering Research*, 65(2). https://doi.org/10.1006/ jaer.1996.0085
- Fowkes, F. M. (1964). Dispersion force contributions to surface and interfacial tensions, contact angles, and heats of immersion. https://doi.org/10.1021/ba-1964-0043.ch006
- Friman Peretz, M., Geoola, F., Yehia, I., Ozer, S., Levi, A., Magadley, E., et al. (2019). Testing organic photovoltaic modules for application as greenhouse cover or shading element. *Biosystems Engineering*, 184. https://doi.org/10.1016/j. biosystemseng.2019.05.003
- Ghasemi Mobtaker, H., Ajabshirchi, Y., Ranjbar, S. F., & Matloobi, M. (2016). Solar energy conservation in greenhouse: Thermal analysis and experimental validation. *Renewable Energy*, 96. https://doi.org/10.1016/j.renene.2016.04.079
- Goetzler, W., Guernsey, M., & Young, J. (2014). Research & development roadmap for emerging HVAC technologies. Retrieved from https://www.energy.gov/eere/buildings/downloads/research-development-roadmap-emerging-hvac-technologies.
- Gorjian, S., Calise, F., Kant, K., Ahamed, M. S., Copertaro, B., Najafi, G., et al. (2021). A review on opportunities for implementation of solar energy technologies in agricultural greenhouses. *Journal of Cleaner Production*. https://doi.org/10.1016/j. jclepro.2020.124807
- Hassanien, R. H. E., Li, M., & Yin, F. (2018). The integration of semi-transparent photovoltaics on greenhouse roof for energy and plant production. *Renewable Energy*, 121. https://doi.org/10.1016/j.renene.2018.01.044
- Ho, J. Y., & Leong, K. C. (2021). A critical review of filmwise natural and forced convection condensation on enhanced surfaces. Applied Thermal Engineering, 186. https://doi.org/10.1016/j.applthermaleng.2020.116437
- Katzin, D., Marcelis, L. F. M., & van Mourik, S. (2021). Energy savings in greenhouses by transition from high-pressure sodium to LED lighting. *Applied Energy*, 281. https:// doi.org/10.1016/j.apenergy.2020.116019
- Kim, S., & Kim, K. J. (2011). Dropwise condensation modeling suitable for superhydrophobic surfaces. *Journal of Heat Transfer*, 133(8). https://doi.org/ 10.1115/1.4003742
- Koh, J. C. Y., Sparrow, E. M., & Hartnett, J. P. (1961). The two phase boundary layer in laminar film condensation. *International Journal of Heat and Mass Transfer*, 2(1–2). https://doi.org/10.1016/0017-9310(61)90015-1
- Kuijpers, W. J. P., Katzin, D., van Mourik, S., Antunes, D. J., Hemming, S., & van de Molengraft, M. J. G. (2021). Lighting systems and strategies compared in an optimally controlled greenhouse. *Biosystems Engineering*, 202. https://doi.org/ 10.1016/j.biosystemseng.2020.12.006
- Kulacki, F. A., Acharya, S., Chudnovsky, Y., Cotta, R. M., Devireddy, R., Dhir, V. K., et al. (2018). Handbook of thermal science and engineering. Handbook of thermal science and engineering. https://doi.org/10.1007/978-3-319-26695-4
- Lemal, D. M. (2004). Perspective on fluorocarbon chemistry. Journal of Organic Chemistry. https://doi.org/10.1021/jo0302556
- Li, D., Yang, R., Arıcı, M., Wang, B., Tunçbilek, E., Wu, Y., et al. (2022). Incorporating phase change materials into glazing units for building applications: Current progress and challenges. Applied Thermal Engineering. https://doi.org/10.1016/j. applithermaleng.2022.118374
- Lund, J. W., & Toth, A. N. (2021). Direct utilization of geothermal energy 2020 worldwide review. *Geothermics*, 90. https://doi.org/10.1016/j. geothermics.2020.101915
- Maeda, K., Tsunetsugu, Y., Miyamoto, K., & Shibusawa, T. (2021). Thermal properties of wood measured by the hot-disk method: Comparison with thermal properties measured by the steady-state method. *Journal of Wood Science*, 67(1). https://doi. org/10.1186/s10086-021-01951-1
- Maraveas, C. (2019). Environmental sustainability of greenhouse covering materials. Sustainability. https://doi.org/10.3390/su11216129
- Maraveas, C., Kotzabasaki, M. I., Bayer, I. S., & Bartzanas, T. (2023). Sustainable greenhouse covering materials with nano- and micro-particle additives for enhanced radiometric and thermal properties and performance. AgriEngineering, 5(3). https://doi.org/10.3390/agriengineering5030085
- Max, J. F. J., Reisinger, G., Hofmann, T., Hinken, J., Tantau, H. J., Ulbrich, A., et al. (2012). Glass-film-combination: Opto-physical properties and energy saving potential of a novel greenhouse glazing system. *Energy and Buildings*, 50. https://doi. org/10.1016/j.enbuild.2012.03.051
- Minkowycz, W. J., & Sparrow, E. M. (1966). Condensation heat transfer in the presence of noncondensables, interfacial resistance, superheating, variable properties, and

- diffusion. International Journal of Heat and Mass Transfer, 9(10). https://doi.org/10.1016/0017-9310(66)90035-4
- Moffat, R. J. (1985). Using uncertainty analysis in the planning of an experiment. *Journal of Fluids Engineering, Transactions of the ASME, 107*(2). https://doi.org/10.1115/
- Murono, T., Kenta Hongo, K. N., & Maezono, R. (2022). Ab-initio-based interface modeling and statistical analysis for estimate of the water contact angle on a metallic Cu(111) surface. Surfaces and Interfaces, 34.
- Neumann, A. W., Abdelmessih, A. H., & Hameed, A. (1978). The role of contact angles and contact angle hysteresis in dropwise condensation heat transfer. *International Journal of Heat and Mass Transfer*, 21(7). https://doi.org/10.1016/0017-9310(78) 90186-2
- Nusselt, W. (1916). Die Oberflächenkondensation des Wasserdampfes. Zeitschrift des Vereins Deutscher Ingenieure, 60.
- Oh, J., Zhang, R., Shetty, P. P., Krogstad, J. A., Braun, P. V., & Miljkovic, N. (2018). Thin film condensation on nanostructured surfaces. Advanced Functional Materials, 28(16). https://doi.org/10.1002/adfm.201707000
- Papadakis, G., Briassoulis, D., Scarascia Mugnozza, G., Vox, G., Feuilloley, P., & Stoffers, J. A. (2000). Review paper (SE—structures and environment): Radiometric and thermal properties of, and testing methods for, greenhouse covering materials. *Journal of Agricultural Engineering Research*, 77(1).
- Pieters, J. G., & Deltour, J. M. (1997). Performances of greenhouses with the presence of condensation on cladding materials. *Journal of Agricultural Engineering Research*, 68 (2). https://doi.org/10.1006/jaer.1997.0187
- Pollet, I. V., & Pieters, J. G. (1999). Condensation and radiation transmittance of greenhouse cladding materials: Part 1, laboratory measuring unit and performance. *Journal of Agricultural Engineering Research*, 74(4). https://doi.org/10.1006/ jaer.1999.0475
- Pollet, I. V., & Pieters, J. G. (2000a). Condensation and radiation transmittance of greenhouse cladding materials, part 2: Results for a complete condensation cycle. *Journal of Agricultural Engineering Research*, 75(1). https://doi.org/10.1006/ jaer.1999.0487
- Pollet, I. V., & Pieters, J. G. (2000b). Condensation and radiation transmittance of greenhouse cladding materials, part 3: Results for glass plates and plastic films. *Journal of Agricultural Engineering Research*, 77(4). https://doi.org/10.1006/ jaer.2000.0628
- Pollet, I. V., & Pieters, J. G. (2002). PAR transmittances of dry and condensate covered glass and plastic greenhouse cladding. Agricultural and Forest Meteorology, 110(4). https://doi.org/10.1016/S0168-1923(01)00295-7
- Poots, G., & Miles, R. G. (1967). Effects of variable physical properties on laminar film condensation of saturated steam on a vertical flat plate. *International Journal of Heat* and Mass Transfer, 10(12). https://doi.org/10.1016/0017-9310(67)90038-5
- Rabiu, A., Na, W. H., Ákpenpuun, T. D., Rasheed, A., Adesanya, M. A., Ogunlowo, Q. O., et al. (2022). Determination of overall heat transfer coefficient for greenhouse energy-saving screen using Trnsys and hotbox. *Biosystems Engineering*, 217. https://doi.org/10.1016/j.biosystemseng.2022.03.002
- Ranjbarzadeh, R., Moradikazerouni, A., Bakhtiari, R., Asadi, A., & Afrand, M. (2019). An experimental study on stability and thermal conductivity of water/silica nanofluid: Eco-friendly production of nanoparticles. *Journal of Cleaner Production*, 206. https://doi.org/10.1016/j.jclepro.2018.09.205
- Reddy, P. P. (2016). Sustainable crop protection under protected cultivation. Sustainable Crop Protection under Protected Cultivation. https://doi.org/10.1007/978-981-287-052.2
- Rose, J. W. (1980). Approximate equations for forced-convection condensation in the presence of a non-condensing gas on a flat plate and horizontal tube. *International Journal of Heat and Mass Transfer*, 23(4). https://doi.org/10.1016/0017-9310(80)

- Rosengarten, G., Cooper-White, J., & Metcalfe, G. (2006). Experimental and analytical study of the effect of contact angle on liquid convective heat transfer in microchannels. *International Journal of Heat and Mass Transfer, 49*(21–22). https://doi.org/10.1016/j.ijheatmasstransfer.2006.02.057
- Sahdev, R. K., Kumar, M., & Dhingra, A. K. (2019). A comprehensive review of greenhouse shapes and its applications. Frontiers in Energy. https://doi.org/10.1007/ s11708-017-0464-8
- Singh, R. D., & Tiwari, G. N. (2010). Energy conservation in the greenhouse system: A steady state analysis. *Energy*, 35(6). https://doi.org/10.1016/j.energy.2010.02.003
- Skarphagen, H., Banks, D., Frengstad, B. S., & Gether, H. (2019). Design considerations for borehole thermal energy storage (BTES): A review with emphasis on convective heat transfer. Geofluids. https://doi.org/10.1155/2019/4961781
- Sparrow, E. M., & Gregg, J. L. (1959). A boundary-layer treatment of laminar-film condensation. *Journal of Heat Transfer*, 81(1). https://doi.org/10.1115/1.4008118
- Sparrow, E. M., Minkowycz, W. J., & Saddy, M. (1967). Forced convection condensation in the presence of noncondensables and interfacial resistance. *International Journal of Heat and Mass Transfer*, 10(12). https://doi.org/10.1016/0017-9310(67)90053-1
- Teitel, M., Vitoshkin, H., Geoola, F., Karlsson, S., & Stahl, N. (2018). Greenhouse and screenhouse cover materials: Literature review and industry perspective. Acta Horticulturae, 1227. https://doi.org/10.17660/ActaHortic.2018.1227.4
- Trosseille, J., Mongruel, A., Royon, L., & Beysens, D. (2022). Effective substrate emissivity during dew water condensation. *International Journal of Heat and Mass Transfer*, 183. https://doi.org/10.1016/j.ijheatmasstransfer.2021.122078
- Vitkin, V., Polishchuk, A., Chubchenko, I., Popov, E., Grigorenko, K., Kharitonov, A., et al. (2020). Raman laser spectrometer: Application to 12C/13C isotope identification in Ch4 and Co2 greenhouse gases. Applied Sciences, 10(21). https://doi.org/10.3390/app10217473
- Wang, J. J., & Beltran, L. (2016). A method of energy simulation for dynamic building envelopes. *Proceedings of SimBuild*, 6(1)
- Wang, J. J., & Shi, D. (2017). Spectral selective and photothermal nano structured thin films for energy efficient windows. Applied Energy, 208, 83–96.
- Wang, Y., Xu, G., Yu, H., Hu, C., Yan, X., Guo, T., et al. (2011). Comparison of anticorrosion properties of polyurethane based composite coatings with low infrared emissivity. *Applied Surface Science*, 257(10). https://doi.org/10.1016/j. apsusc.2010.12.152
- Xie, J., Wang, W., Sang, P., & Liu, J. (2018). Experimental and numerical study of thermal performance of the PCM wall with solar radiation. *Construction and Building Materials*, 177. https://doi.org/10.1016/j.conbuildmat.2018.05.123
- Yang, S. H., Lee, C. G., Ashtiani-Araghi, A., Kim, J. Y., & Rhee, J. Y. (2015). Heat gain and contribution to heating from supplemental lighting in greenhouse. *Engineering in Agriculture, Environment and Food*, 8(2), https://doi.org/10.1016/j.eaef.2015.04.001
- Yano, A., & Cossu, M. (2019). Energy sustainable greenhouse crop cultivation using photovoltaic technologies. *Renewable and Sustainable Energy Reviews*. https://doi. org/10.1016/j.rsep.2019.04.026
- Yilmaz, Z., & Çetintaş, F. (2005). Double skin façade's effects on heat losses of office buildings in Istanbul. *Energy and Buildings*, 37(7). https://doi.org/10.1016/j. enbuild.2004.07.010
- Zhang, E., Duan, Q., Wang, J., Zhao, Y., & Feng, Y. (2021). Experimental and numerical analysis of the energy performance of building windows with solar NIR-driven plasmonic photothermal effects. *Energy Conversion and Management*, 245, 114594.
- Zhang, E., Jahid, M. A., & Wang, J. (2023). Evaluation of six greenhouse covering materials for energy performance. In *In proceedings of the American solar energy* society national conference (pp. 13–20). Springer Nature Switzerland.
- Zhu, Y., Li, Y., Ding, H., Lu, A., Li, Y., & Wang, C. (2021). Multifactor-controlled mid-infrared spectral and emission characteristic of carbonate minerals (MCO3, M = Mg, Ca, Mn, Fe). *Physics and Chemistry of Minerals*, 48(4). https://doi.org/10.1007/s00269-021-01140-y